Journal of Biomedical Optics

BiomedicalOptics.SPIEDigitalLibrary.org

Label-free detection and characterization of the binding of hemagglutinin protein and broadly neutralizing monoclonal antibodies using terahertz spectroscopy

Yiwen Sun
Junlan Zhong
Cunlin Zhang
Jian Zuo
Emma Pickwell-MacPherson

SPIE.

Label-free detection and characterization of the binding of hemagglutinin protein and broadly neutralizing monoclonal antibodies using terahertz spectroscopy

Yiwen Sun,[a,*] Junlan Zhong,[a] Cunlin Zhang,[b] Jian Zuo,[b] and Emma Pickwell-MacPherson[c,*]
[a]Shenzhen University, School of Medicine, National-Regional Key Technology Engineering Laboratory for Medical Ultrasound, Guangdong Key Laboratory for Biomedical Measurements and Ultrasound Imaging, Department of Biomedical Engineering, Shenzhen 518060, China
[b]Capital Normal University, Department of Physics, Beijing 100037, China
[c]Chinese University of Hong Kong, Department of Electronic Engineering, Shatin, Hong Kong

Abstract. Hemagglutinin (HA) is the main surface glycoprotein of the influenza A virus. The H9N2 subtype influenza A virus is recognized as the most possible pandemic strain as it has crossed the species barrier, infecting swine and humans. We use terahertz spectroscopy to study the hydration shell formation around H9 subtype influenza A virus's HA protein (H9 HA) as well as the detection of antigen binding of H9 HA with the broadly neutralizing monoclonal antibody. We observe a remarkable concentration dependent nonlinear response of the H9 HA, which reveals the formation process of the hydration shell around H9 HA molecules. Furthermore, we show that terahertz dielectric properties of the H9 HA are strongly affected by the presence of the monoclonal antibody F10 and that the terahertz dielectric loss tangent can be used to detect the antibody binding at lower concentrations than the standard ELISA test.
[DOI: 10.1117/1.JBO.20.3.037006]

Keywords: terahertz spectroscopy; label-free; hemagglutinin; antigen–antibody interaction; dielectric property.

Paper 140795PR received Dec. 2, 2014; accepted for publication Feb. 16, 2015; published online Mar. 10, 2015.

1 Introduction

Influenza (flu) is a respiratory infection in mammals and birds: it is a major medical problem and a constant threat to human health. Influenza viruses are characterized by the two types of surface antigen hemagglutinin (HA) and neuraminidase that they carry,[1] e.g., H1N1, H5N2. HA protein comprises 516 amino acids and has the predicted molecular mass of 58.2 kDa. Based on the HA sequences, there are at least 16 different HA subtypes (H1-H16) of the influenza A virus by various combinations of HA, as shown in Fig. 1(a). The virus H9N2 subtype influenza A is recognized as the most possible pandemic strain as it was prevalent in poultry in Southeast Asia and has crossed the species barrier, also infecting swine and humans.[2] After the isolation of the H9N2 virus from two human cases in Hong Kong since 1999, the H9 subtype influenza A virus and its HA protein (H9 HA) have attracted significant attention.[3–5] HA protein comprises over 80% of the envelope proteins present in the virus particle and is involved in two major functions: recognition of target cells by binding to their sialic acid-containing receptors and fusion of the viral and the endosomal membranes succeeding endocytosis.[6]

Fully human monoclonal antibody F10 is an HA-specific broadly neutralizing monoclonal antibody (nAb).[7] From the crystal structure of F10-bound HA, the heavy chain (VH) of antibody F10 inserts its heavy chain into a conserved pocket in the neck (stem region) of HA, which blocks membrane fusion and prevents productive infection by diverse influenza A viruses. H9 HA is a trimer-forming glycoprotein [Fig. 1(b)] which contributes three conserved hydrophobic epitopes and one F10 nAb binds into each epitope in the HA-antibody complex as shown in Fig. 1(c).[7–10]

The HA-antibody reaction leads to a rich phenomenology that is essential in diagnostics studies. Many methods, such as immunofluorescence,[11] enzyme-linked immunosorbent assay (ELISA),[1] western blotting,[11,12] chemiluminescence immunoassay,[13] and immuno-polymerase chain reaction,[14] are widely used to study such interactions. However, all of them are used as labeled methods. In ELISA, for instance, the antibody is linked to an enzyme as a molecular label, and a substance containing the enzyme's substrate is used to detect the bound enzyme, most commonly by a color change in the substrate.

Terahertz time-domain spectroscopy (THz-TDS) techniques allow us to obtain both amplitude and phase information. By Fourier transform of the time-domain waveform, the absorption coefficient n(ω) and refractive index a(ω) can be simultaneously obtained. These can then be used to calculate the complex permittivity $\varepsilon^*(\omega) = \varepsilon'(\omega) - i\varepsilon'(\omega)$ in which the real part ε' corresponds to the dielectric constant and the imaginary part ε'', known as the dielectric loss factor, is a measure of the energy absorption per cycle.[15] THz absorption spectra are very sensitive to crystalline structures of molecules.[16,17] However, in amorphous systems, spectrally localized features

*Address all correspondence to: Yiwen Sun, E-mail: ywsun@szu.edu.cn or Emma Pickwell-MacPherson, E-mail: emma@ee.cuhk.edu.hk;

1083-3668/2015/$25.00 © 2015 SPIE

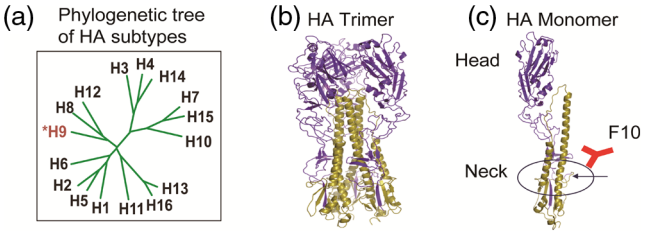

Fig. 1 (a) Phylogenetic tree of the 16 influenza A virus subtypes; (b) structure of hemagglutinin (HA) protein. HA is a trimer consisting of three identical copies of the HA protein; (c) binding model of antibody F10 with H9 HA monomer.

are usually not observed in the THz range because of the strong coupling between the random environment and the intramolecular modes.[18] Dielectric spectroscopy provides a simple, label-free and sensitive approach for many protein investigations.[19] With the advent of pulsed THz-TDS techniques, low frequency dielectric characterization of proteins can be accomplished. For example, the nonlinear absorption properties of proteins (e.g., ubiquitin, λ*6-86 protein and bovine serum albumin) in the terahertz range have been reported by the groups of Ebbinghaus et al. and Bye et al.[20,21]

THz dielectric spectroscopy has been used to investigate proteins as the protein macromolecules can be considered as dipole and their orientation significantly affects their THz dielectric response.[22] Their orientation can also be controlled by an external THz electric field: the transition dipole moments are aligned with the THz field and lead to effective dielectric heterogeneities. To probe the antibody–antigen reaction, the dielectric properties can be obtained from the transmitted THz pulse through a sample, as the THz vibrational frequencies associated with these rearrangement motions are largely determined by the forces (e.g., hydrogen bonding, electrostatic, van der Waals, hydrophobic bonds) which were responsible for the antibody–antigen binding.[23–26] The specificity and sensitivity of antibody–antigen interactions are fundamental for understanding the biological activity of these proteins and motivate further fundamental research on nAb-based high-sensitivity drug screening and pharmaceuticals for influenza viruses. This work presents the first THz time-domain spectroscopy investigation of the immune response of the HA protein (H9 HA) with its specific and nonspecific antibodies (F10 nAb/irmAB). Our findings showed enhanced sensitivity compared to those achieved by the ELISA test which is currently widely used in biomedical and clinic settings.

2 Materials and Methods

2.1 *Spectroscopy System*

Terahertz spectra were acquired using a commercial Z-3™ Time-Domain THz spectrometer (Zomega THz Corp., Troy, United States). In this system, optical excitation is achieved by a mode-locked Mai-Tai laser which emits fewer than 120 fs pulses centered at a wavelength of 800 nm, with an 80 MHz repetition rate and an average power of ~1 W. The measurements were conducted in the typical transmission geometry at room temperature (~298 K), the optics were purged using nitrogen gas to remove the water vapor from the air to decrease the humidity down to less than 1%. The usable frequency range of the system is from about 0.1 to 2.5 THz, but the valid range tends to decrease when the sample is in an aqueous phase due to signal attenuation by the sample.

2.2 *Sample Holder*

The sample holder was fabricated from TOPAS™ 5013L-10. This material (which is a cyclic olefin co-polymer) was chosen because it has very low attenuation at THz frequencies.[27] The hydrated protein formulation was pipetted into the sample holder with a liquid layer which is of the order of a few micrometers thick for the THz measurement. The clean homogeneous empty sample cell was also measured as a reference (refractive index ~1.53) enabling the spectroscopic properties of the sample to be accurately determined. Each ample was measured four times. For each measurement, the sample was extracted and repipetted in the sample holder. By averaging the spectra, systematic errors produced by wrong positioning, as well as present heterogeneities in the sample, were minimized.

2.3 *Protein and Monoclonal Antibody Preparation*

The recombinant HA protein was purchased from Sino Biological (Cat no. 11229-V08H). Briefly, the DNA sequence encoding the extracellular domain of influenza A virus (A/HongKong/1073/1999; H9N2) HA was synthesized and expressed in human embryonic kidney 293 cells. The recombinant HA protein was not infectious and had no biohazard risk for any *in-vitro* study. Fully human monoclonal antibody F10 was expressed in 293T cells using TCAE5.3 vector[28] containing corresponded immunoglobulin heavy chain (VH) and light chain (VL) gene and purified using protein A beads (GE Healthcare). The concentration of the proteins was determined using the Protein A280 application module by NanoDrop spectrophotometer (Thermo Scientific). Fully human anti-CXCR4 monoclonal antibody (purchased from NBGen) was used as the irrelevant antibody control (irmAb) in this study. All of the H9 HA, F10 antibodys and irmAb were stored in sterilized phosphate-buffered saline (PBS) at pH 7.4. H9 HA was prepared at the following concentration using PBS as diluents: 7.5, 15, 29, 56, 113, 225 and 430 μg/ml.

2.4 *Enzyme Linked Immunosorbent Assay*

The 100 μl H9 HA from each concentration was coated in the ELISA plate at 4°C overnight, followed by adding 100 μl of the F10 antibody in each well. After 1 h incubation at room temperature, the plate was intensively washed using phosphate buffered saline with Tween20 (PBST). Then the HRP conjugated goat anti-human IgG mAb was used as a secondary antibody for color development. For different concentrations of coated H9 HA, PBS and irmAb were used as the negative and irrelevant control. Optical density (OD) values of 450 nm were read and results were expressed as the OD reading at different H9 HA concentrations. All protein related experiments were performed by NBGen laboratory using the indicated methods.

3 Results and Discussion

We have measured the THz properties of H9 HA, H9-F10 and H9/irmAb and performed an ELISA test on H9-F10, H9/irmAb and PBS. In the following sections, we report our data and the analysis resulting from these measurements.

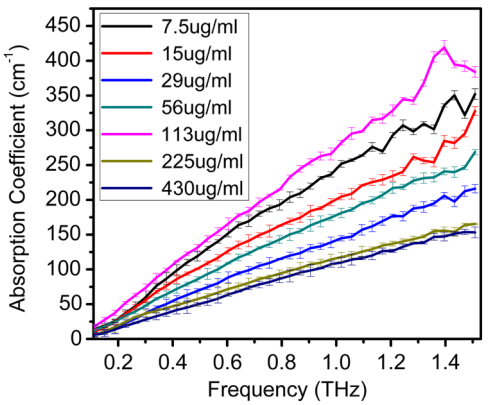

Fig. 2 Absorption coefficients of H9 HA solution at concentrations from 7.5 to 430 μg/ml. Error bars represent 95% confidence intervals.

3.1 *HA H9 Protein*

The liquid phase of the H9 HA protein lacked any distinct peaks in the spectral region studied as shown in Fig. 2. Together with the average over multiple measurements, the 95% confidence intervals are plotted as error bars to determine whether differences are statistically significant. For each concentration, the absorption increases with increasing frequency. However, the absorption coefficient does not simply decrease with increasing protein concentration. Instead there is a more complex relationship.

We see in Fig. 2 that the absorption coefficient for the 113 μg/ml solution is higher than for all the other concentrations between 7.5 and 430 μg/ml. The absorption coefficient for the 29 μg/ml solution is also seemingly out of sequence. To highlight these features and illustrate how the absorption coefficient depends on both frequency and concentration, we have plotted the absorption coefficients against concentration for H9 HA from 0.26 to 1.47 THz in Fig. 3.

If the protein solution followed the Beer–Lambert law, then the absorption coefficient a(ω) would be a linear function with increasing protein concentration. However, from Fig. 3, we see that the absorption coefficient decreases with increasing H9 HA concentration up to 29 μg/ml. Then, between concentrations of 29 and 113 μg/ml, the absorption coefficient increases, reaching its maximum at 113 μg/ml. As the concentration increases further, the absorption coefficient decreases. This remarkable "zig-zag" behavior of the absorption coefficient can be explained by considering the protein interactions present

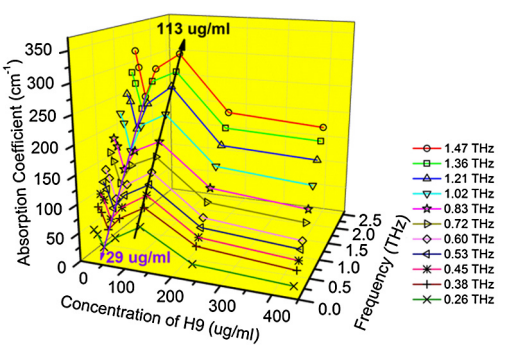

Fig. 3 Dependence of the absorption coefficient of H9 HA on protein concentration between 0.1 and 1.5 THz.

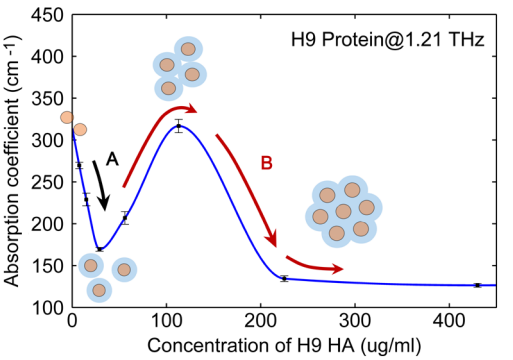

Fig. 4 The absorption coefficient of H9 HA at 1.21 THz as a function of concentration. The schematic molecules illustrate the formation and overlap of the hydration shells to interpret the nonlinear absorption behaviors. Region A follows a binary component model and a Region B follows a ternary component model.

at different concentrations. At the lower concentrations (7.5 to 29 μg/ml), there is no dynamical hydration shell around the H9 HA molecules. The absorption coefficient of bulk water in the terahertz region is much higher than that of the protein, so as the H9 HA concentration increases, the absorption coefficient decreases (region A of Fig. 4). This continues until the hydration shell starts to form at around 29 μg/ml. The absorption of the hydration shell in the terahertz region is greater than that of the bulk water and as the protein concentration increases further, the absorption coefficient increases (start of region B of Fig. 4). This continues until the hydration shells start to overlap at about 113 μg/ml: the overlapping causes the absorption coefficient to decrease again, and it continues to decrease until the shells become saturated at about 225 μg/ml and the absorption plateaus. Thus, the behavior for region A (black arrow in Fig. 4) could be modeled as a two component model (protein and bulk water)[29] and the behavior in region B (red arrow in Fig. 4) could be modeled by a ternary component model (protein, hydration water and bulk water). This assumes a distinct absorption coefficient of the water around the solute molecule due to the distinct properties of the solvation water.[30] By using the concentration at which the hydration shells become saturated, we calculate the hydration shell to be 8.84 Å. This result corresponds to about two to three hydration water shells around a HA protein molecule (~3 Å average extension per water molecule) which is similar to previously reported results.[29–31]

3.2 *H9-F10 Binding Reaction*

To investigate the protein binding reaction, F10 nAb (230 μg/ml, ~160 KD) was mixed into H9 HA solutions with the concentration from 7.5 to 430 μg/ml by 1:1 volume ratio. The irmAb was used as the negative control with the same reaction molar ratio. The mixtures were incubated with gentle mixing for ~30 min at room temperature and then overnight at 4°C to allow binding reactions and complex formation. No precipitate was observed in the samples.

Table 1 presents the reaction ratio of the H9 HA binding F10 nAb in our study. As explained in Sec. 1, usually ~3 antigen-binding fragments (Fabs) per trimer H9 HA can saturate all the F10 binding sites. This gives an optimum ratio of binding sites for H9:F10 as 1:1 and 1:3 for $H9_{trimer}$: F10. To investigate the relationship between THz absorption and concentration, we chose the concentration of the F10 such that the optimum

Table 1 H9 hemagglutinin (HA) binding F10 antibody reaction ratio.

F10 (μg/ml)	H9 monomor (μg/ml)	Ratio of binding sites (H9: F10)	Molar ratio ($H9_{trimer}$:F10)	
	7.5	0.09:1	0.09:3	F10 excess
	15	0.18:1	0.18:3	
	29	0.35:1	0.35:3	
230	56	0.67:1	0.67:3	
	113	1.35:1	1.35:3	H9 excess
	225	2.69:1	2.69:3	
	430	5.14:1	5.14:3	

ratio would occur when the concentration of H9 HA is nearly 113 μg/ml.

To obtain a full picture of how the absorption coefficient depends on both frequency and concentration, we present the 3-D plots of the concentration-dependent terahertz absorption for the H9 HA binding F10 nAb [Fig. 5(a)] and the irmAb [Fig. 5(b)] in the range of 0.1 to 1.5 THz. We use the RBS H9-F10 values instead of the protein concentration as it accounts for the concentrations of both F10 and H9 HA. Figure 5(c) uses the data at 1.21 THz to highlight the comparison of absorption properties against the RBS of H9-F10 and H9/irmAb solutions. In the spectral range from 0.1 to 1.5 THz, we have observed a remarkable absorption of H9 HA solutions at 113 μg/ml because of the overlap of the hydration shell. Within our measurement for antibody/antigen mixtures, the absorption property has been similarly shown in H9/irmAb groups (negative control) but shifted to the smaller concentration of 56 μg/ml. However, the effect of the hydration shell was not present in the H9 HA binding F10 (red solid line) in Fig. 5(c). This is because the HA protein contains a large number of amino and carboxyl residues (e.g., COO^-), which charged the surface of the protein in neutral solutions. Polarized water molecules and oppositely charged sites on antibodies (e.g., NH^{3+}) shape the hydration shell around the protein by electrostatics. The binding interactions between antibodies and antigens cause the charged sites to reduce and even disappear. Consequently, the hydration shell becomes lose. As for the negative control group, there is no binding interaction between the H9 HA and irmAb molecules, and the hydration shells overlap at a lower concentration than for H9 HA because of the higher molecular density. The terahertz spectroscopy data for the H9-F10 indicate that the absorption coefficient decreases sharply with an increasing ratio of the binding sites of H9/F10 until about 1.35, which is the closest to the optimum ratio (see also Table 1). After that, the absorption coefficient increases gradually by reason of the excess of the H9 HA in solution.

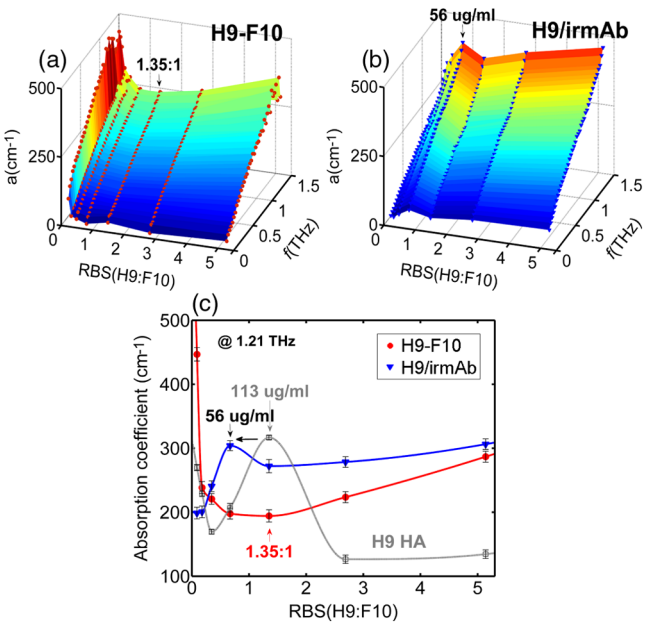

Fig. 5 The concentration dependence of the absorption coefficient for (a) H9-F10 solution and (b) negative control (H9/irmAb) at frequencies 0.1 to 1.5 THz. (c) Plot of concentration against absorption coefficient of H9, H9/irmAb and H9-F10 solution at 1.21 THz. (RBS: ratio of binding sites).

3.3 *Specificity and Sensitivity Detection for the H9-F10 Binding*

The dielectric loss tangent is defined by $\tan\delta = \varepsilon''/\varepsilon'$, which quantifies a dielectric material's inherent dissipation of electromagnetic energy to charge motion. Moreover, $\tan\delta$ measurements are extremely sensitive to protein molecular relaxation and local motions involving the reorientation of side-chains of residues as it is subjected to an oscillating electric field.[32] This enables us to detect the specificity and sensitivity of antibody–antigen binding using THz spectroscopy. In Fig. 6, we show the Cole–Cole plots (ε' versus ε'') for our data.

H9 HA has such a higher dielectric constant and dielectric loss compared to the H9/irmAb mixtures that the H9 HA group and the H9/irmAb group are clearly separated in the

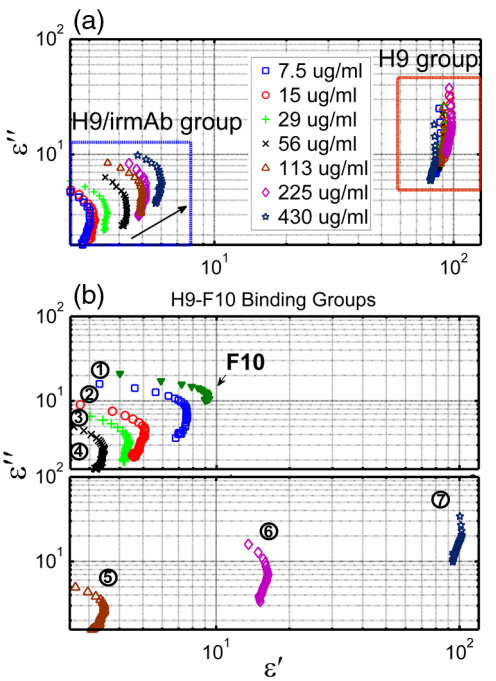

Fig. 6 Cole–Cole plots for (a) H9 HA solution, mixtures of H9 HA and irmAb and (b) H9 HA binding F10 nAb at different concentrations.

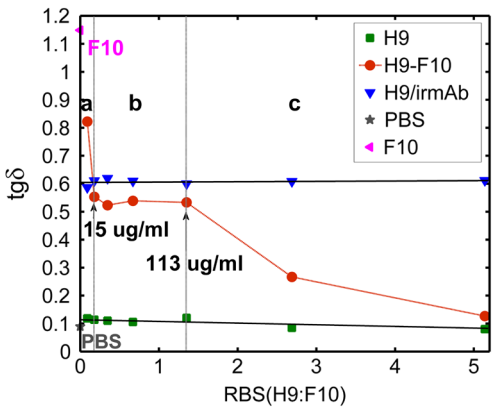

Fig. 7 Plot of tan δ versus ratio of binding sites of H9 HA and F10 (red circle) and negative control (blue down arrow), H9 HA solutions presented by green marks for the comparison. F10 nAb solution has the higher dielectric loss tangent of about 1.18 (pink left arrow) and PBS solutions with the weakest polar characteristics indicate the lowest tan δ of about 0.1 (dark gray star). The linear best fit is also shown (black solid line) for H9 and H9/irmAb.

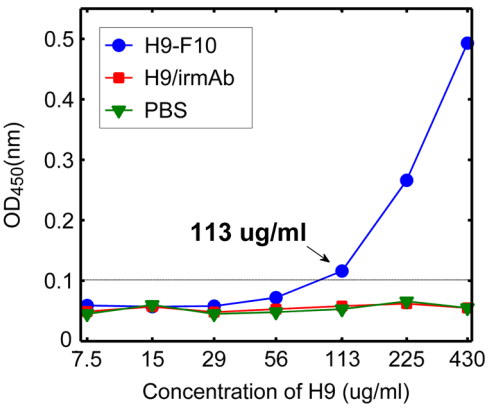

Fig. 8 Specificity and sensitivity measurements by ELISA. OD_{450} is the optical density at 450 nm.

plot. The Cole–Cole plots for H9/irmAb mixtures are close to semicircular arcs. However, for the H9 HA, the data shape can be described as a skewed arc, indicating a distribution of relaxation times for these samples. Furthermore, it is interesting to find that for the distribution of H9-F10 binding complex in Cole–Cole plots, the values for the imaginary and real parts initially decreased from the range of H9/irmAb (concentrations 1 to 4) and then increased up to the range of H9 HA (concentrations 5 to 7) with the F10 nAb consumed.

Figure 7 shows the relationship between the dielectric loss tangent and the reaction concentrations of H9-F10 and H9/irmAb at 1.21 THz, respectively. The H9 solution is plotted by green marks for comparison. All H9 HA, H9-F10 complex solutions and H9/irmAb mixtures display polar polymer characteristics as they have a relatively large dielectric loss tangent (0.1 or more). PBS solution has the weakest polar characteristics and had the lowest tanδ of about 0.1 (dark gray star). The results indicate that the tan δ values of H9 HA and H9/irmAb solutions are approximately independent of concentration and lie at 0.12 and 0.61, respectively, for a wide range of concentrations. However, the dielectric loss tangent of the H9-F10 solutions (red line) was found to have three significant stages. At stage (a), increasing the H9 HA content in a fixed concentration of F10 nAb caused the tanδ values to decrease sharply. This is because the F10 nAb solution has a higher dielectric loss tangent of about 1.18 (pink mark) and the reaction molar ratio of H9 HA and F10 in solutions is smaller than F10 itself at the beginning. After a relatively steady stage (b) during which the dielectric loss tangent remains close to 0.53, the magnitude of tanδ decreases again and approaches the value for the H9 HA solution of about 0.12, stage (c). From these results, we can deduce that the binding state of the antigen with its specific antibody is detected at stage (b) as the dielectric loss tangent reaches a stable stage which means an energy balance of antigen–antibody interaction. Stage (b) starts at 15 μg/ml, therefore, this is the minimum detectable limit of H9-F10 binding in our work. The nonlinear change in the dielectric loss tangent observed at 113 μg/ml occurs at the same concentration at which the hydration shells of H9 HA started to overlap in Fig. 3 and is caused by the excess of the H9 HA as per the analysis in Table 1.

3.4 *ELISA for H9-F10 Binding*

An ELISA test was performed to determine the specificity and sensitivity of antigen binding events between H9 HA and F10 nAb. In Fig. 8, the result showed that while there was no observed binding of PBS and irmAb with H9 HA at each concentration, F10 was detected to bind to the H9 HA with increasing concentration. The ELISA test results were considered positive when the OD was >0.1 over the negative control. Here, the gradually escalated signal could be observed in the F10 binding curve (blue) starting at a concentration of 113 μg/ml: they surged after that, which indicated that the detection limit determined by ELISA for H9-F10 was 113 μg/ml compared to 15 μg/ml with the terahertz dielectric loss tangent. Thus, the standard ELISA test is not as sensitive to the binding as the terahertz dielectric loss tangent.

4 Conclusion

In this paper, we have employed terahertz spectroscopy to probe the binding of HA protein H9 with an HA-specific broadly neutralizing monoclonal antibody F10. From our THz measurements, we observed that the hydration shell is always present in the charged H9 HA and H9/irmAb solutions, but that the binding interaction between H9 HA and F10 nAb effectively causes the hydration shell to disappear. This highlights that binding sites of the antibody–antigen affect the configuration of the protein such that it can be detected by THz spectroscopy. The dielectric loss tangent provided a sensitive approach to monitor the H9-F10 interaction: the detection limit was 15 μg/ml for H9 HA compared to 113 μg/ml for the ELISA test.

Our measurements of H9 HA with an HA-specific broadly neutralizing monoclonal antibody F10 highlight the unique capabilities of THz spectroscopy for probing antibody–antigen binding label-free. This provides motivation for further investigation into the potential to use of THz spectroscopy as a promising strategy for nAb-based high-sensitivity drug screening and pharmaceutical applications in the future.

Acknowledgments

The authors gratefully acknowledge partial financial support for this work from the National Natural Science Foundation of China (No. 61205092 and 11204190); the Foundation for Distinguished Young Talents in Higher Education of Guangdong, China (No. 2012LYM_0116); the Guangdong Natural Science Foundation (No. S2012040007668); Nanshan Core Technology

Breakthrough Project (No. KC2013JSJS0003A) and the Research Grants Council of Hong Kong (No. 415313). We thank Dr. Yong Liu for his assistance in figures of the structure of the HA protein drawing. We also express our sincere thanks to NBGen laboratory for sample synthesis and preparation.

References

1. J. H. Sui et al., "Structural and functional bases for broad-spectrum neutralization of avian and human influenza A viruses," *Nat. Struct. Mol. Biol.* **16**, 265–273 (2009).
2. T. Horimoto and Y. Kawaoka, "Pandemic threat posed by avian influenza A viruses," *Clin. Microbiol. Rev.* **14**, 129–149 (2001).
3. M. Peiris et al., "Human infection with influenza H9N2," *Lancet* **354**, 916–917 (1999).
4. Y. Guan et al., "Molecular characterization of H9N2influenza viruses: were they the donors of the"internal"genes of H5N1viruses in Hong Kong?," *Proc. Natl. Acad. Sci. USA* **96**, 9363–9367 (1999).
5. M. Peiris et al., "Influenza A H9N2: aspects of laboratory diagnosis," *J. Clin. Microbiol.*, **37** 3426–3427 (1999).
6. J. M. White et al., "Attachment and entry of influenza virus into host cells. Pivotal roles of hemagglutinin," in W. Chiu, R. M. Burnett, and R. L. Garcea, *Structural Biology of Viruses*, pp. 80–104, Oxford University Press, New York (1997).
7. D. C. Ekiert et al., "Antibody recognition of a highly conserved influenza virus epitope: implications for universal prevention and therapy," *Science* **324**, 246–251 (2009).
8. A. K. Kashyap et al., "Combinatorial antibody libraries from survivors of the Turkish H5N1 avian influenza outbreak reveal virus neutralization strategies," *Proc. Natl. Acad. Sci. USA* **105**, 5986–5991 (2008).
9. D. C. Ekiert et al., "A highly conserved neutralizing epitope on group 2 influenza A viruses," *Science* **333**, 843–850 (2011).
10. D. Corti et al., "A neutralizing antibody selected from plasma cells that binds to group 1 and group 2 influenza A hemagglutinins," *Science* **333**, 850–856 (2011).
11. R. Hai et al., "Influenza viruses expressing chimeric hemagglutinins: globular head and stalk domains derived from different subtypes," *J. Virol.* **86**, 5774–5781 (2012).
12. J. Steel et al., "Influenza virus vaccine based on the conserved hemagglutinin stalk domain," *mBio* **1**, e00018 (2010).
13. M. W. Henderson et al., "Contribution of bordetella filamentous hemagglutinin and adenylate cyclase toxin to suppression and evasion of interleukin-17-mediated inflammation," *Infect. Immun.* **80**, 2061–2075 (2012).
14. A. S. Mweene et al., "Development of immuno-PCR for diagnosis of bovine herpesvirus 1 infection," *J. Clin. Microbiol.* **34**, 748–750 (1996).
15. R. Pethig, "Protein-water interactions determined by dielectric methods," *Annu. Rev. Phys. Chem.* **43**, 177–205 (1992).
16. P. F. Taday, I. V. Bradley, and D. D. Arnone, "Terahertz pulse spectroscopy of biological materials: L-Glutamic acid," *J. Biol. Phys.* **29**, 109–115 (2003).
17. P. F. Taday et al., "Using terahertz pulse spectroscopy to study the crystalline structure of a drug: a case study of the polymorphs of ranitidine hydrochloride," *J. Pharm. Sci.* **92**, 831–838 (2003).
18. P. U. Jepsen and S. J. Clark, "Precise ab-initio prediction of terahertz vibrational modes in crystalline systems," *Chem. Phys. Lett.* **442**, 275–280 (2007).
19. H. Betting et al., "Investigation of aqueous alcohol and sugar solutions with reflection terahertz time-domain spectroscopy," *Phys. Chem. Chem. Phys.* **3**, 1688–1692 (2001).
20. S. Ebbinghaus et al., "An extended dynamical hydration shell around proteins," *Proc. Natl. Acad. Sci. USA* **104**, 20749–20752 (2007).
21. J. W. Bye et al., "Analysis of the hydration water around bovine serum albumin using terahertz coherent synchrotron radiation," *J. Phys. Chem. A* **118**, 83–88 (2014).
22. D. V. Matyushov, "Terahertz response of dipolar impurities in polar liquids: On anomalous dielectric absorption of protein solutions," *Phys. Rev. E*, **81**, 021914 (2010).
23. B. Born et al., "Solvation dynamics of model peptides probed by terahertz spectroscopy. Observation of the onset of collective network motions," *J. Am. Chem. Soc.* **131**, 3752–3755 (2009).
24. B. Born et al., "The terahertz dance of water with the proteins: the effect of protein flexibility on the dynamical hydration shell of ubiquitin," *Faraday Discuss.* **141**, 161–173 (2009).
25. A. Markelz et al., "THz time domain spectroscopy of biomolecular conformational modes," *Phys. Med. Biol.* **47**, 3797–3805 (2002).
26. R. Singh et al., "Improved mode assignment for molecular crystals through anisotropic terahertz spectroscopy," *J. Phys. Chem. A* **116**, 10359–10364 (2012).
27. J. Balakrishnan, B. M. Fischer, and D. Abbott, "Sensing the hygroscopicity of polymer and copolymer materials using terahertz time-domain spectroscopy," *Appl. Opt.* **48**, 2262–2266 (2009).
28. M. E. Reff et al., "Depletion of B cells in vivo by a chimeric mouse human monoclonal antibody to CD20," *Blood* **83**, 435–445 (1994).
29. Y. W. Sun, Y. T. Zhang, and E. Pickwell-MacPherson, "Investigating antibody interactions with a polar liquid using terahertz pulsed spectroscopy," *Biophys. J.* **100**, 225–231 (2011).
30. U. Heugen et al., "Solute-induced retardation of water dynamics probed directly by terahertz spectroscopy," *Proc. Natl. Acad. Sci. U. S. A.* **103**, 12301–12306 (2006).
31. Y. W. Sun et al., "Observing the temperature dependent transition of the GP2 peptide using terahertz spectroscopy," *PLoS One* **7**, e50306 (2012).
32. R. A. Broglia, L. Serrano, and G. Tiana, *Protein Folding and Drug Design*, pp. 193–206, IOS Press, Canada (2007).

Yiwen Sun is an associate professor at Shenzhen University. She received her BS degree in optical information science and technology from Xidian University in 2004, and then graduated from the Institute of Optoelectronics, Shenzhen University, with a Master of Physical Electronics in 2007. She then began a PhD program with the Terahertz Group at the Chinese University of Hong Kong (HK), investigating the potential applications of terahertz radiation. She received the PhD degree in 2010. Her current research interests are focused on understanding the dielectric response in biosystems by probing kinetics of reactions with terahertz radiation.

Emma Pickwell-MacPherson set up the first terahertz laboratory in Hong Kong at the Chinese University of Hong Kong (CUHK) in 2007. She is known for her biomedical-related research in the terahertz community. She represents Hong Kong, China, on the International Organising Committee for the Infrared, Millimetre and Terahertz Waves conference series and will chair the conference to be held at CUHK in 2015.

Biographies of the other authors are not available.